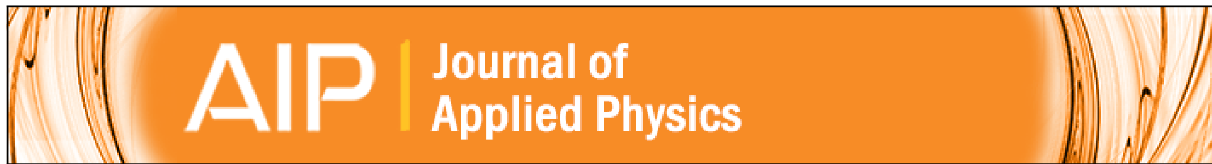

On the microstructure of Si coimplanted with H + and He + ions at moderate energies

S. Reboh, F. Schaurich, A. Declemy, J. F. Barbot, M. F. Beaufort, N. Cherkashin, and P. F. P. Fichtner

Citation: Journal of Applied Physics **108**, 023502 (2010); doi: 10.1063/1.3459884
View online: http://dx.doi.org/10.1063/1.3459884
View Table of Contents: http://scitation.aip.org/content/aip/journal/jap/108/2?ver=pdfcov
Published by the AIP Publishing

Articles you may be interested in

Formation process of β - Fe Si 2 ∕Si heterostructure in high-dose Fe ion implanted Si
J. Appl. Phys. **99**, 113527 (2006); 10.1063/1.2201729

Mechanism of the Smart Cut™ layer transfer in silicon by hydrogen and helium coimplantation in the medium dose range
J. Appl. Phys. **97**, 083527 (2005); 10.1063/1.1865318

Evolution of hydrogen and helium co-implanted single-crystal silicon during annealing
J. Appl. Phys. **90**, 3780 (2001); 10.1063/1.1389478

Transient enhanced diffusion and defect microstructure in high dose, low energy As + implanted Si
J. Appl. Phys. **84**, 5997 (1998); 10.1063/1.368896

Microstructural difference between platinum and silver trapped in hydrogen induced cavities in silicon
Appl. Phys. Lett. **72**, 2713 (1998); 10.1063/1.121108

MIT LINCOLN LABORATORY CAREERS

Discover the satisfaction of innovation and service to the nation

- Space Control
- Air & Missile Defense
- Communications Systems & Cyber Security
- Intelligence, Surveillance and Reconnaissance Systems
- Advanced Electronics
- Tactical Systems
- Homeland Protection
- Air Traffic Control

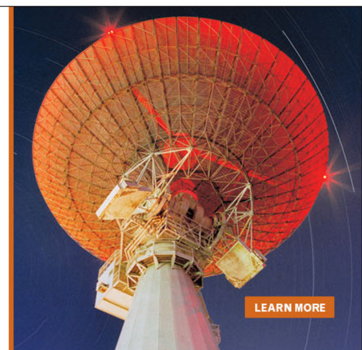

[This article is copyrighted as indicated in the article. Reuse of AIP content is subject to the terms at: http://scitation.aip.org/termsconditions. Downloaded to] IP: 143.54.162.138 On: Tue, 19 May 2015 18:48:40

JOURNAL OF APPLIED PHYSICS **108**, 023502 (2010)

On the microstructure of Si coimplanted with H^+ and He^+ ions at moderate energies

S. Reboh,[1,2,a)] F. Schaurich,[3] A. Declemy,[4] J. F. Barbot,[4] M. F. Beaufort,[4] N. Cherkashin,[2] and P. F. P. Fichtner[3]

[1]*PGCIMAT, Universidade Federal do Rio Grande do Sul, 91501-970 Porto Alegre, Brazil*
[2]*Groupe nMat, CEMES-CNRS, 29 rue J. Marvig, 31055 Toulouse, France*
[3]*Escola de Engenharia, Universidade Federal do Rio Grande do Sul, 91501-970 Porto Alegre, Brazil*
[4]*PHYMAT-CNRS, Université de Poitiers, 86962 Futuroscope, France*

(Received 1 May 2010; accepted 3 June 2010; published online 19 July 2010)

We report on the microstructure of silicon coimplanted with hydrogen and helium ions at moderate energies. X-ray diffraction investigations in as-implanted samples show the direct correlation between the lattice strain and implanted ion depth profiles. The measured strain is examined in the framework of solid mechanics and its physical origin is discussed. The microstructure evolution of the samples subjected to intermediate temperature annealing (350 °C) is elucidated through transmission electron microscopy. Gas-filled cavities in the form of nanocracks and spherical bubbles appear at different relative concentration, size, and depth location, depending on the total fluence. These different microstructure evolutions are connected with the surface exfoliation behavior of samples annealed at high temperature (700 °C), determining the optimal conditions for thick layer transfer. 1.5 μm thick Si films are then obtained onto glass substrates. © *2010 American Institute of Physics*. [doi:10.1063/1.3459884]

I. INTRODUCTION

The fracture engineering of semiconducting materials implanted with hydrogen ions allows the transfer of single crystalline thin films onto host substrates.[1,2] It basically consists in the implantation of H^+ into a target substrate, producing a localized concentration that exceeds its solid solubility limit. The ballistic character of the implantation process also creates a high density of point defects and the undergoing microstructure modification generates a considerable lattice strain.[3–5] Hence, H-implanted substrates are thermodynamically unstable and the supply of thermal energy leads to the coprecipitation of H and vacancies in the form of nanosized crack-like cavities, mainly lying parallel to the surface.[4] The preferential nanocrack orientation plays a crucial role in the layer transfer process and is related to an interplay between cavity nucleation and lattice strain.[4,6] Nanocrack evolves thermally via Ostwald ripening[7] and subcritical crack propagation[8] and the complete overlayer separation is achieved when cracks coalescence sweeps the whole substrate.[1,2]

This process was originally conceived using H,[1] however, the total amount of ions to activate the process is considerably reduced by coimplanting H and He.[9,10] This effect has been attributed to a synergy between the H-chemistry, that stabilizes the internal surface of the crack and breaks the Si–Si bond at the crack-tip, and the efficient crack pressurization provided by He.[8–10] Although the main physic concept of the coimplantation has been realized, it is a complex system for which the microstructure evolution strongly depends on experimental parameters, as the implantation order, energy range, and relative depth positions of H and He depth profiles.[11]

More recently, the investigation of moderate implantation energy of H^+ and He^+ in Si, leading to micrometer-scale depth penetration of the ions, provided significant information on fracture mechanism culminating in the layer separation, demonstrating also the possibility to obtain freestanding films.[12] Furthermore, the development of a method to obtain and integrate single crystalline semiconducting films of micrometer-thicknesses is of great interest for thin-film solar cells fabrication. In this context, a series of recent breakthroughs conducting to record energy conversion were achieved using multilayered structures.[13,14] However, the integration of materials with significant lattice mismatch has been the main challenge in this field and is still limiting further improvements.

Here, we study the effects of $H^+ + He^+$ coimplantation in the microstructure of (001) Si substrates, in connection with the development of micrometer-thick layer transfer. We start by investigating the strain in as-implanted samples, showing that the strain intensity enhances and the deformed region enlarges with increasing fluence. The depth-distribution of strain is found to be related to the implanted ions depth profile. An evolving contribution of H and He occurs for different fluences and the physical origin of strain is discussed. The microstructure developments after intermediate temperature annealing (350 °C) are examined and correlated with the strain distribution in the as-implanted state and with the surface exfoliation behavior upon high temperature annealing (700 °C). The optimal fluence conditions for thick layer transfer via H+He coimplantation are found, and a Si layer of 1.5 μm thickness is obtained onto a glass substrate.

[a)]Electronic mail: shay.reboh@cemes.fr.

 © 2010 American Institute of Physics

[This article is copyrighted as indicated in the article. Reuse of AIP content is subject to the terms at: http://scitation.aip.org/termsconditions. Downloaded to] IP: 143.54.162.138 On: Tue, 19 May 2015 18:48:40

II. EXPERIMENTAL

Czochralsky grown p-type (001) Si substrates with a resistivity of 1–25 Ω cm, were implanted with H^+ ions at 168 keV, followed by He^+ ions at 345 keV, respecting a 1H/1He ratio. The chosen energies provided coincident projected ion range at ≈1500 nm depth from the wafer surface.[15] Three samples were implanted at distinct total fluence Φ_T ($\Phi H^+ + \Phi He^+$) of 2, 6, and 10×10^{16} cm^{-2}, referred further as low fluence (LF), intermediate fluence (IF), and high fluence (HF), respectively. The implantations were carried out at room temperature, with the samples 7° off-axis and controlled current densities ≤0.5 μA cm^{-2}. Thermal annealing of the samples was performed in high vacuum, either at 350 or 700 °C during 1800 s, to, respectively, study the microstructure evolution and surface exfoliation behavior of the samples.

As-implanted samples were characterized by x-ray diffraction (XRD). ($\theta/2\theta$) scans in the vicinity of the (004) reflection of Si allowed to determine the lattice strain gradient in the direction normal to the sample surface.[5,12] The experiments were performed in an automated two circles goniometer, using a Cu $K_{\alpha1}$ radiation provided by a 5 kW RIGAKU RU-200 source with a vertical linear focus in combination with a quartz monochromator. The XRD curves were simulated combining ion implantation[15] and XRD[16] codes.

Microstructure investigation after 350 °C annealing was carried out by transmission electron microscopy (TEM) in a JEOL 2010 microscope, operating at 200 kV. The surface characterization of the samples upon 700 °C annealing was conducted by scanning electron microscopy (SEM) in a JEOL JSM-5800.

Samples implanted according to the parameters leading to optimized exfoliation were bonded onto glass substrates by hydrophobic surface activation[17] and annealed up to 600 °C to obtain layer separation. The transferred films were characterized by TEM.

III. RESULTS

A. As-implanted samples

Figure 1 displays the XRD curves obtained from the three implanted samples and a reference curve from a pristine substrate. All curves exhibit a main diffraction peak at $2\theta_B\approx69.14°$ rising from the undamaged crystal. For the implanted samples, the scattered intensity producing interference fringe patterns for $\theta<2\theta_B$ is characteristic of a tensile strain gradient of Gaussian-like shape.[5] The maximum strain (ε_{max}), given by the position of the last fringe away from the Bragg peak, increases with the fluence. For the LF sample, $\varepsilon_{max}\approx0.5\%$. For IF and HF samples, ε_{max} could not be determined due to the decreasing intensity diffracted by the highly strained region, which falls below the detection limit of the experiment. The drop of the intensity is related to the rising concentration of lattice damage.[18] However, the reduction in the fringes spacing with increasing fluence points out the widening of the strain profile.[5]

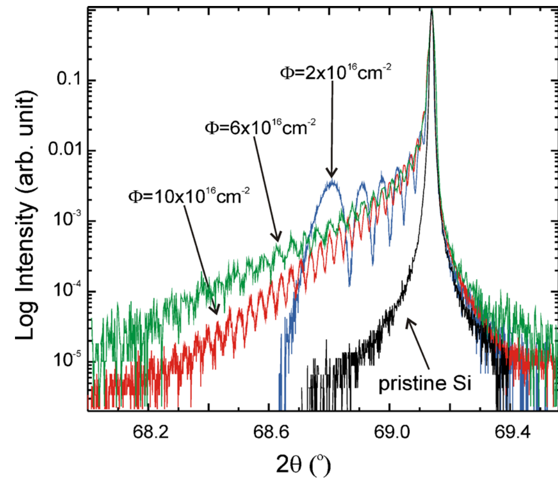

FIG. 1. (Color online) ($\theta/2\theta$) XRD scans close to the (004) reflection of Si obtained from the samples implanted to Φ_T=2, 6, and 10×10^{16} cm^{-2} and a reference curve from a pristine sample.

B. Intermediate temperature annealing (350 °C and 1800 s)

Figure 2 presents low magnification cross-section TEM micrographs of the samples annealed at 350 °C. The accumulated lattice damage appears as diffuse darker regions (under bright-field diffraction contrast). The superimposed curves correspond to the ion and damage depth profiles estimated by the SRIM (Ref. 15) code. These curves are clearly centered on the damage features observed by TEM. With increasing fluence, the damage distribution widens toward the surface, enlarging from ≈85 nm at LF up to ≈330 nm for IF and ≈360 nm for HF. Figure 3 presents higher magnification images of the damaged layers. For LF [Fig. 3(a)], nanocrack structures, observed in edge-on perspective, present diameters ranging from 30 to 80 nm and form within a narrow depth-distribution ≈80 nm wide. For IF [Fig. 3(b)], the nanocrack diameter is smaller, sizing from 15 to 45 nm and the depth-distribution widens to ≈120 nm. The majority of the damaged region is formed by small spherical bubbles,

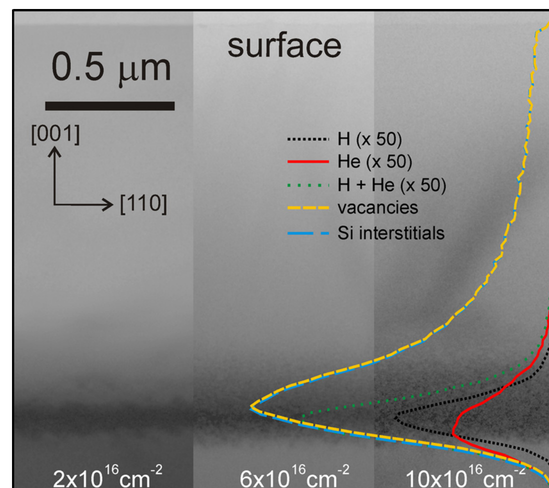

FIG. 2. (Color online) Low magnification cross sectional TEM micrographs of the samples implanted to Φ=2, 6, and 10×10^{16} cm^{-2} and annealed at 350 °C for 1800 s. The superimposed curves are the calculated profiles of the implanted ions and lattice damage.

[This article is copyrighted as indicated in the article. Reuse of AIP content is subject to the terms at: http://scitation.aip.org/termsconditions. Downloaded to] IP: 143.54.162.138 On: Tue, 19 May 2015 18:48:40

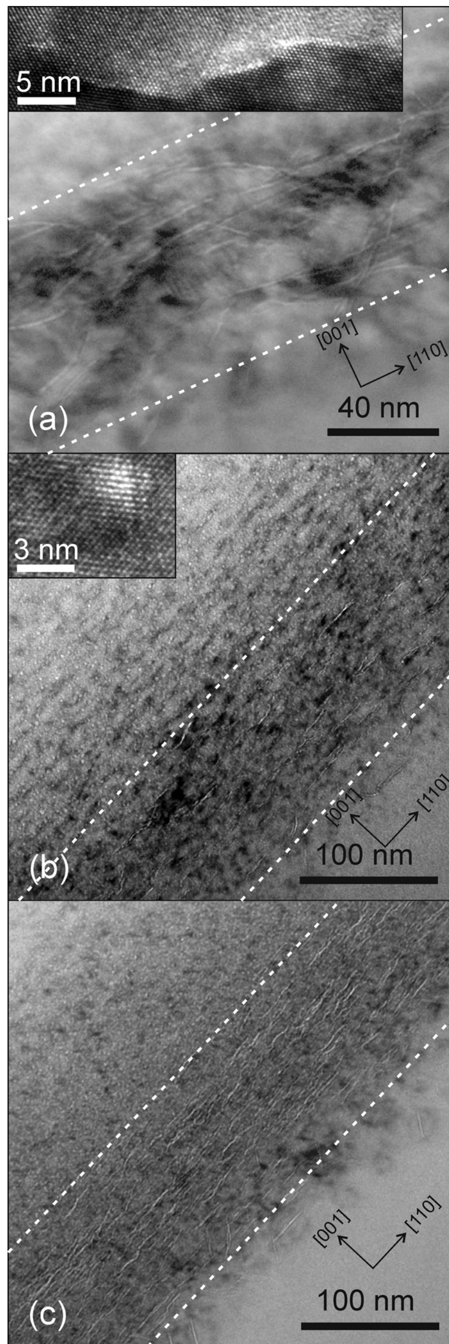

FIG. 3. High magnification cross sectional TEM micrographs of samples implanted to (a) $\Phi=2\times10^{16}$ cm^{-2}, (b) $\Phi=6\times10^{16}$ cm^{-2}, and (c) $\Phi=10\times10^{16}$ cm^{-2} annealed at 350 °C for 1800 s. The insets in the figure show a detailed image of a nanocrack (a) and a spherical cavity (b). The region between the dotted lines indicates the extension within the implanted layer that effectively contains nanocracks.

with diameters ranging from 1 to 4 nm. Bubbles are observed in a region extending from the nanocracks layer up to ≈210 nm toward the surface. For the HF sample [Fig. 3(c)], the width of the nanocracks region is similar to the IF sample but the region containing bubbles widens. No significant modification of the typical cavity size is observed. Regardless of the fluence, the distribution of nanocracks is centered at ≈1530 nm depth, close to the projected range of the implanted ions.

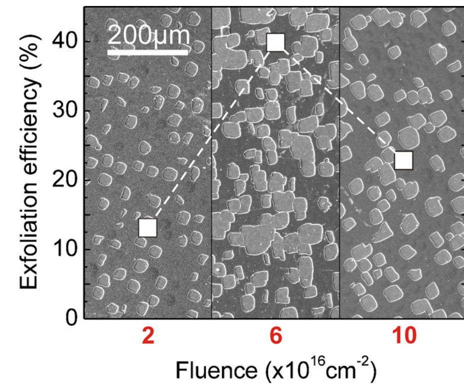

FIG. 4. (Color online) SEM micrographs of the samples annealed at 700 °C during 1800 s. The exfoliation efficiency values are plotted as a function of the total fluence superimposed to the respective sample image.

C. High temperature annealing (700 °C and 1800 s)

The exfoliation behavior of high temperature annealed samples was quantified in terms of an exfoliation efficiency parameter A_{ex}, defined as the fraction of exfoliated area over the specimen area. The obtained values are plotted in Fig. 4, superimposed to SEM image of the corresponding sample. The trend of the curve characterizes an interval of fluences leading to optimal exfoliation. For the present experimental conditions, the maximum $A_{ex}\approx 40\%$ occurs for 6×10^{16} cm^{-2} (i.e., IF). Samples implanted to IF were then hydrophobically bonded onto a glass substrate and annealed up to 600 °C to obtain layer transfer. Figure 5 shows a cross-section TEM micrograph of the transferred film having an estimated thickness of 1530 ± 10 nm.

IV. DISCUSSIONS

Strain in ion implanted semiconductors originates from microscopic lattice defects that behave as point sources introducing isotropic intrinsic strain ε^*.[19] Along the directions parallel to the surface (defined as x and y), the substrate stiffness causes an elastic reaction $e_{yy}=e_{xx}=-\varepsilon^*$, resulting in unchanged lattice parameter. Thus, the relaxation of the lattice occurs along the z direction, i.e., toward the free surface, where $\sigma_{zz}=0$. Therefore, the out-of-plane strain measured by

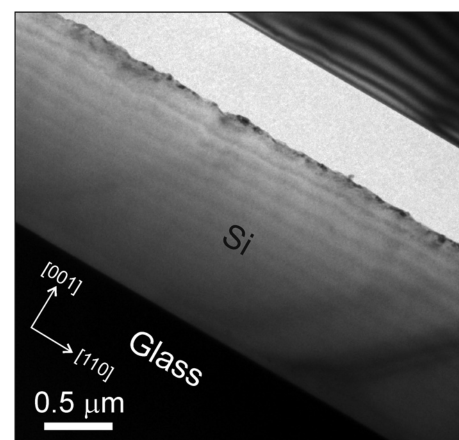

FIG. 5. Cross sectional TEM micrograph of a ≈1.5 μm thick Si film transferred onto a glass substrate.

[This article is copyrighted as indicated in the article. Reuse of AIP content is subject to the terms at: http://scitation.aip.org/termsconditions. Downloaded to] IP: 143.54.162.138 On: Tue, 19 May 2015 18:48:40

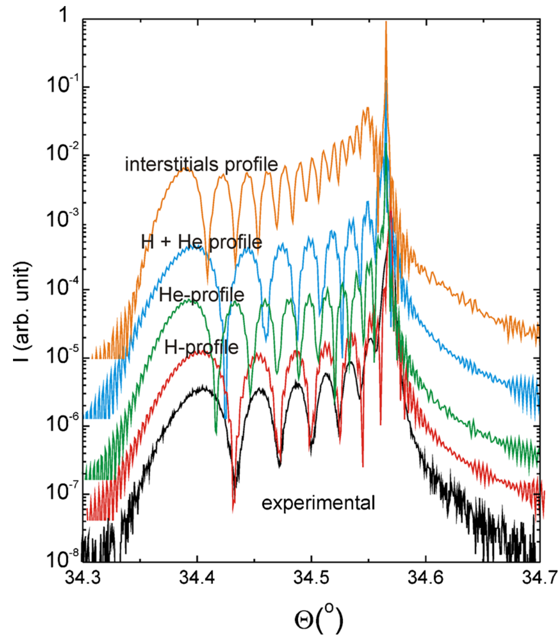

FIG. 6. (Color online) Simulated and experimental XRD curves for the IF sample ($\Phi_T=2\times10^{16}$ cm^{-2}).

XRD is the sum of intrinsic and elastic strains written as $\varepsilon_{zz}=e_{zz}+\varepsilon^*=(\delta d/d)_z$. The elastic component is introduced by the compressive in-plane stress $\sigma^{\text{in-plane}}=\sigma_{yy}=\sigma_{xx}$ given by

$$\sigma^{\text{in-plane}}=-2\mu\left(\frac{\delta d}{d}\right)_Z, \tag{1}$$

where μ is the shear modulus of the substrate (≈68 GPa for Si).

The physical origin of the intrinsic strain is complex and depends on the implanted specie, its chemical-physical interaction with the matrix and with the created lattice damage.[20] Generally, in addition to the implanted atoms, the collision cascade produced by the incident ions mostly creates vacancies and self-interstitials in the matrix. Self-interstitial atoms introduce tensile strain in the lattice,[21] and, in opposition, vacancies generate compressive strain.[20] For medium and heavy ions implantation, such individual effects are clearer due to the reasonable spatial separation between vacancy, ion, and interstitial profiles.[20–22] In the case of light ions as H^+ and He^+, the closer location of damage and ion profiles renders a more intricate system. The approach adopted here to get an insight on the physical origin of strain is to first identify its characteristic depth-distribution. As the XRD measurements are not sensitive neither to the depth position nor to the symmetry of the profile,[5] the reconstruction of strain distributions from the experimental curves is not straightforward, as it has multiple solutions. Thus, the experimental curves were tentatively calculated assuming that the strain profile follows the simulated depth-concentrations of: (i) H atoms; (ii) He atoms; (iii) integrated H+He atoms; and (iv) self-interstitials. The more precise calculations were conducted for the LF sample for which the complete strain profile was accurately measured. Figure 6 presents the results along with the experimental curve. For this fluence, the simulations show that the shape of the measured strain distribution is intimately related to the H-distribution. Accordingly, the in-plane stress in the sample can be described replacing the $(\delta d/d)_z$ factor in Eq. (1) by a Gaussian function $G(z)$ given by

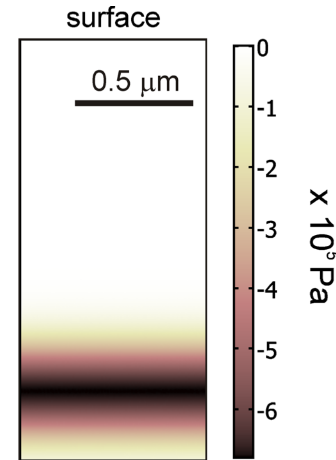

FIG. 7. (Color online) Calculated distribution of compressive in-plane stress in the LF sample ($\Phi=2\times10^{16}$ cm^{-2}).

$$G(z)=\left(\frac{\delta d}{d}\right)_Z^{\text{MAX}} e^{\left(-\frac{(z-R_p)^2}{2\Delta R_p^2}\right)}. \tag{2}$$

In Eq. (2), $(\delta d/d)_Z^{\text{MAX}}$ is the maximum out-of-plane strain along z and R_p and ΔR_p are the mean range and full width at half maximum of the H-distribution. Figure 7 presents the calculated stress of the LF sample. The maximum stress value is about 0.7 GPa.

Albeit the shape of the strain distribution for the LF sample is related to the H-distribution, the strain intensity is higher than what is expected for the implantation of 10^{16} H/cm^{-2} in Si.[23] This demonstrates an effective contribution of He, which takes place within the previously implanted H-profile. Upon annealing at 350 °C, this sample only presented nanocracks confined in narrow layer (see Fig. 3), further indicating an effective interaction of He with the H-rich region, as has been reported for low energy implants.[24]

For the IF and HF samples, the as-implanted strain significantly widens and the simulation of the XRD curves (not shown) indicated a rising contribution of the He-related depth-distribution as the fluence increase. This result can be discussed in connection with the depth-distribution of cavities found upon 350 °C annealing. The broadening of the cavity distribution was observed to be largely dominated by the formation of spherical bubbles above the nanocrack layer (i.e., toward the surface, see Fig. 3). This heterogeneous microstructure can be interpreted in terms of ion and vacancy depth-distributions. According to the simulated profiles shown in Fig. 2, the H+He concentration is peaked at ≈1540 nm depth, close to the observed nanocrack depth location at ≈1530 nm. The vacancy distribution is peaked at a shallower depth of ≈1480 nm and largely extends toward the surface, indicating that spherical bubbles form preferentially in the vacancy-rich region of the damaged layer. This observation agrees with the concept that spherical bubbles result from the combination of gas atoms with a substantial amount

[This article is copyrighted as indicated in the article. Reuse of AIP content is subject to the terms at: http://scitation.aip.org/termsconditions. Downloaded to] IP: 143.54.162.138 On: Tue, 19 May 2015 18:48:40

of vacancies, whereas plate-shape cavities form preferentially under low vacancies availability.[25,26] A competitive behavior for the consumption of gas atoms and vacancies can also explain the smaller nanocracks size concomitantly with the appearance of bubbles. Furthermore, as spherical-shape bubble formation is characteristic of He implantation in Si,[27] it is speculated that in the present case it contains preferentially He atoms. Consequently, the significant widening of the strain profile is related to both the spreading of the implanted region caused by the higher implanted fluence and to an increasing contribution of the expected He depth-distribution, which is initially wider than for H.

The general trend observed in the coimplanted samples is that the strain distribution is directly related to the implanted ion profiles. This implies that significant interstitials and vacancies recombination render the damage contribution negligible out of the implanted ions profile. In the narrow region with high concentration of H and He, gas-vacancy complexes and small cavities readily form during implantation.[27–30] The local consumption of vacancies also avoids interstitials annihilation which, in turn, can be stabilized by H up to high temperature.[30] Hydrogen also forms a weakly bonded structure at the bond centered (BC) and antibonding (AB) site of the Si lattice.[28] However, this configuration stands only for as-implanted state vanishing at low temperature annealing. Differently, the contribution of He in the measured strain can only be attributed to gas-vacancy complexes.[31] Thus, the physical origin of the strain in the as-implanted substrates cannot be assigned to a single type of defect but to a multiple contribution from pressurized gas-vacancy complexes, self-interstitials, and hydrogen atoms at the BC and AB positions of the lattice. Determining the particular contribution of each type of defect remains challenging and it certainly evolves upon annealing.

The exfoliation behavior of the samples submitted to high temperature annealing (Fig. 4) showed the existence of a range of fluences which enhances the surface exfoliation. The reduced exfoliation under LF conditions can be attributed to the low amount of gas atoms involved in the process. Naturally, with increasing fluence the exfoliation is enhanced due to the higher content of gas atoms. However above a given fluence, unfavorable microstructure developments reduce the exfoliation efficiency. In the present case, it was observed the formation/evolution of spherical bubbles competing with nanocracks. The absence of localized surface deformation also implies that the strain induced by the cracks development is somehow relaxed by other mechanisms, such as localized plastic deformation. Plasticity effects in nanocrack-tip have been predicted by calculations[32] and more recently, a mechanism of stress relaxation via plastic-regime interaction of nanocracks was observed.[8] Those phenomena may be favored in highly damaged substrates.

Finally, wafer bonding and Si layer transfer onto glass substrate was carried out using the implantation condition leading to optimal exfoliation efficiency (IF, $\Phi_T = 6 \times 10^{16}$ cm^{-2}, see Fig. 4). The film thickness of $\approx$1530 nm (see Fig. 5) shows that the fracture process occurred along the region of maximum nanocrack concentration. The absence of treading dislocations in the transferred film for such combination of materials with considerably distinct thermal expansion, show that the method can be further explored to obtain good quality micron-scale semiconducting materials integration.

V. CONCLUSION

In summary, the microstructure of H+He coimplanted Si was studied by XRD, TEM, and SEM. The strain distribution measured by XRD in as-implanted samples was found to be intimately related to the implanted ion depth profiles. For LF, the H-distribution shapes the strain profile and the contribution of He occurs within the region previously implanted with H. For higher fluence this interaction is less effective and an increasing contribution of the He-profile was observed. The physical origin of strain was attributed to multiple contributions from pressurized gas-vacancy complexes, stabilized self-interstitials and hydrogen atoms at the BC and AB positions of the lattice. Upon annealing at intermediate temperature (350 °C), TEM investigations revealed the formation of crack-like and spherical cavities, being their occurrence and depth-distribution strongly dependent on the fluence and ion/damage interaction. The surface exfoliation behavior of the samples was studied upon high temperature annealing (700 °C), showing that IFs lead to optimal conditions for layer transfer. LFs produce low exfoliation efficiency due to the low amount of gas atoms participating in the process. HFs generate unfavorable microstructure. Finally, using the optimized implantation fluence, Si films $\approx$1.5 μm thick were transferred onto a glass substrate. The development of micron-scale thick layer transfer provides a method to integrate semiconducting films for high efficiency solar cells fabrication.

ACKNOWLEDGMENTS

The authors acknowledge the support of the Brazilian agencies CAPES (Process BEX 2358/09-3) and CNPq, PETROBRAS S.A. and the Center for Electron Microscopy (CME) of the Universidade Federal do Rio Grande do Sul (UFRGS).

[1] M. Bruel, Mater. Res. Innovations **3**, 9 (1999).
[2] B. Aspar, H. Moriceau, E. Jalaguier, C. Lagahe, A. Soubie, B. Biasse, A. M. Papon, A. Claverie, J. Grisolia, G. Benassayag, F. Letertre, O. Rayssac, T. Barge, C. Maleville, and B. Ghyselen, J. Electron. Mater. **30**, 834 (2001).
[3] T. Höchbauer, A. Misra, M. Nastasi, and J. W. Mayer, J. Appl. Phys. **92**, 2335 (2002).
[4] M. Nastasi, T. Höchbauer, J.-K. Lee, A. Misra, J. P. Hirth, M. Ridgway, and T. Lafford, Appl. Phys. Lett. **86**, 154102 (2005).
[5] N. Sousbie, L. Capello, J. Eymery, F. Rieutorda, and C. Lagahe, J. Appl. Phys. **99**, 103509 (2006).
[6] S. Reboh, M. F. Beaufort, J. F. Barbot, J. Grilhé, and P. F. P. Fichtner, Appl. Phys. Lett. **93**, 022106 (2008).
[7] J. Grisolia, G. Ben Assayag, A. Claverie, B. Aspar, C. Lagahe, and L. Laanab, Appl. Phys. Lett. **76**, 852 (2000).
[8] S. Reboh, J. F. Barbot, M. F. Beaufort, and P. F. P. Fichtner, Appl. Phys. Lett. **96**, 031907 (2010).
[9] A. Agarwal, T. E. Haynes, V. C. Venezia, O. W. Holland, and D. J. Eaglesham, Appl. Phys. Lett. **72**, 1086 (1998).
[10] M. K. Weldon, M. Collot, Y. J. Chabal, V. C. Venezia, A. Agarwal, T. E. Haynes, D. J. Eaglesham, S. B. Christman, and E. E. Chaban, Appl. Phys. Lett. **73**, 3721 (1998).
[11] P. Nguyen, K. K. Bourdelle, T. Maurice, N. Sousbie, A. Boussagol, X.

[This article is copyrighted as indicated in the article. Reuse of AIP content is subject to the terms at: http://scitation.aip.org/termsconditions. Downloaded to] IP: 143.54.162.138 On: Tue, 19 May 2015 18:48:40

Hebras, L. Portigliatti, F. Letertre, A. Tauzin, and N. Rochat, J. Appl. Phys. **101**, 033506 (2007).
[12]S. Reboh, A. A. de Mattos, J. F. Barbot, A. Declemy, M. F. Beaufort, R. M. Papaléo, C. P. Bergmann, and P. F. P. Fichtner, J. Appl. Phys. **105**, 093528 (2009).
[13]J. F. Geisz, S. Kurtz, M. W. Wanlass, J. S. Ward, A. Duda, D. J. Friedman, J. M. Olson, W. E. McMahon, T. E. Moriarty, and J. T. Kiehl, Appl. Phys. Lett. **91**, 023502 (2007).
[14]J. F. Geisz, D. J. Friedman, J. S. Ward, A. Duda, W. J. Olavarria, T. E. Moriarty, J. T. Kiehl, M. J. Romero, A. G. Norman, and K. M. Jones, Appl. Phys. Lett. **93**, 123505 (2008).
[15]J. F. Ziegler, J. P. Biersack, and U. Littmark, *The Stopping and Range of Ions in Solids* (Pergamon, New York, 1985).
[16]S. A. Stepanov, http://sergey.gmca.aps.anl.gov/
[17]Q. Y. Tong and U. Gösele, *Semiconductor Wafer Bonding: Science and Technology* (Wiley, New York, 1999).
[18]P. H. Dederichs, J. Phys. F: Met. Phys. **3**, 471 (1973).
[19]J. Qu and M. Cherkaoui, *Fundamentals of Micromechanics of Solids* (Wiley, New York, 2006).
[20]J. P. de Souza, Y. Suprun-Belevich, H. Boudinov, and C. A. Cima, J. Appl. Phys. **87**, 8385 (2000).
[21]S. Koffel, N. Cherkashin, F. Houdellier, M. J. Hytch, G. Benassayag, P. Scheiblin, and A. Claverie, J. Appl. Phys. **105**, 126110 (2009).
[22]Y. Zhong, C. Bailat, R. S. Averback, S. K. Ghose, and I. K. Robinson, J. Appl. Phys. **96**, 1328 (2004).
[23]D. Bisero, F. Corni, S. Frabboni, R. Tonini, G. Ottaviani, and R. Balboni, J. Appl. Phys. **83**, 4106 (1998).
[24]X. Duo, W. Liu, M. Zhang, L. Wang, C. Lin, M. Okuyama, M. Noda, W.-Y. Cheung, P. K. Chu, P. Hu, S. X. Wang, and L. M. Wang, J. Phys. D: Appl. Phys. **34**, 477 (2001).
[25]P. F. P. Fichtner, J. R. Kaschny, R. A. Yankov, A. Mucklich, U. Kreibig, and W. Skorupa, Appl. Phys. Lett. **70**, 732 (1997).
[26]M. Hartmann and H. Trinkaus, Phys. Rev. Lett. **88**, 055505 (2002).
[27]X. Hebras, P. Nguyen, K. K. Bourdelle, F. Letertre, N. Cherkashin, and A. Claverie, Nucl. Instrum. Methods Phys. Res. B **262**, 24 (2007).
[28]M. K. Weldon, V. E. Marsico, Y. J. Chabal, A. Agarwal, D. J. Eaglesham, J. Sapjeta, W. L. Brown, D. C. Jacobson, Y. Caudano, S. B. Christman, and E. E. Chaban, J. Vac. Sci. Technol. B **15**, 1065 (1997).
[29]B. Terreault, Phys. Status Solidi A **204**, 2129 (2007).
[30]W. Düngen, R. Job, Y. Ma, Y. L. Huang, T. Mueller, W. R. Fahrner, L. O. Keller, J. T. Horstmann, and H. Fiedler, J. Appl. Phys. **100**, 034911 (2006).
[31]G. F. Cerofolini, F. Corni, S. Frabboni, C. Nobili, G. Ottaviani, and R. Tonini, Mater. Sci. Eng. **27**, 1 (2000).
[32]J. G. Swadener, M. I. Baskes, and M. Nastasi, Phys. Rev. Lett. **89**, 085503 (2002).

[This article is copyrighted as indicated in the article. Reuse of AIP content is subject to the terms at: http://scitation.aip.org/termsconditions. Downloaded to] IP: 143.54.162.138 On: Tue, 19 May 2015 18:48:40